Monografías Matemáticas *García de Galdeano* **40**, 115–124 (2016)

A MODEL FOR RELATIVE EVOLUTION OF 0 AND 1, THE 2 FIXED POINTS OF MULTIPLICATION

Mariá Monserrat Rincon-Camacho

Abstract. We study the fixed-point equation, given for a fixed $l > 0$ by:

$$x = h(1 - |2x - 1|^l), \quad x,\ h \in \mathbb{R},$$

where $|2x - 1| = \frac{|x - \frac{1}{2}|}{\frac{1}{2}}$ represents the relative distance of x to the mean value of 0 and 1 which are the fixed points of multiplication. The particular cases $l = 1$ and 2 are classical. This work intends to look at the question: "How much of the specific behaviour for $l = 1$ and 2 remains valid when the exponent l varies freely in $]0, \infty[$?". Some preliminary answers are given, which are derived either from theory ($l \in \mathbb{N}^*$, $1 \leq l \leq 5$) or from numerical simulation ($0 < l < 1$ or $l > 5$).

Keywords: Fixed points 0 and 1 for real multiplication, relative distance to the mean, logistic family, path of homogenisation, degree of heterogeneity, symbiosis, wavetracks, backward and forward chaos, laws of composition.

AMS classification: 08A02, 37C25, 65P99.

§1. Introduction

1.1. Fixed points of multiplication

Through history, multiplication has been the source of paradoxes leading to the creation of new concepts whenever $x \times x = x^2$ does not behave as expected. The solution of the quadratic equation $x^2 = 2$ defied the law of rationality of ancient Greece, since $\sqrt{2}$ cannot be expressed as the ratio of two integers. Solving $x^2 + 1 = 0$ presented a new obstacle in the 16th century. The solution $\sqrt{-1}$ proposed by Cardano in (1545) provoked resistance during three centuries since it broke the assumed law that a square is positive. For more information about the art of computing and the paradoxes in logic see [3, 4, 5, 16].

Multiplication appears as the *driving force* behind the historical evolution of computation. Over $\mathbb{R}$, the fixed points of $x \times x = x$ are 0 and 1 which define the classical binary logic of Aristotle modelled by the field $\mathbb{Z}_2 = \{0, 1\}$. In this work we aim to model a *real* nonlinear evolution of this classical logic by means of the composition of continuous functions interpreted below as a *nonlinear* generalisation of multiplication. Let $f, g \in C^0(\mathbb{R})$ and consider the law of composition defined as

$$f \circ g = f(g(\cdot)), \quad f, g : \mathbb{R} \mapsto \mathbb{R}.$$

The two fixed points of $f \circ f = f$ are given by the identity function $\mathbf{1} : x \mapsto x$ and the null function $\mathbf{0} : x \mapsto 0$, where: $\mathbf{1} \circ f = f \circ \mathbf{1} = f$ and $\mathbf{0} \circ f = \mathbf{0}$, $f \circ \mathbf{0} = f(0) \not\equiv \mathbf{0}$. If there is no

ambiguity with numerical exponentiation, we denote $f \circ f$ as f^2, $f^k = f \circ (f^{k-1})$, $k \geq 1$ and $f^0 = \mathbf{1}$. It is possible to interpret the relation $f^2 = f$ for $\circ$ as a nonlinear generalisation of $x^2 = x$ for $\times$. If f is the linear map $x \mapsto a \times x$, then $\circ$ reduces to $\times$, see [11], but in general $\circ$ is neither commutative nor distributive with respect to $+$. Thus, the multiplicative law given by $\circ$ endows the Banach space $C^0(\mathbb{R})$ with a *nonlinear* generalisation of multiplication. Over linear functions, the functions $\mathbf{0}$ and $\mathbf{1}$ are characterised by the numbers 0 and 1 by the obvious identities: $\mathbf{1} : x \mapsto x = 1 \times x$ and $\mathbf{0} : x \mapsto 0 = 0 \times x$.

The composition of functions as a multiplicative law can be illustrated by studying a fixed-point equation of the type

$$x = f_h(x), \quad h \in \mathbb{R} \tag{1}$$

where the real parameter h induces an evolution. Indeed, it has been experimentally shown that many evolutive physical phenomena in Nature are adequately explained by the dynamic evolution present in (1), see [12, 17]. As an example of (1), here we propose to study the following fixed-point equation which is based on the *relative* distance $|2x - 1|$ to the mean value $\frac{1}{2} = \frac{0+1}{2}$ between 0 and 1

$$x = h(1 - |2x - 1|^l), \quad x, \ h \in \mathbb{R}. \tag{2}$$

1.2. Scope of the paper

Most of the numerical and theoretical studies about (2) have focussed on the classical cases $l = 2$ (mostly) and $l = 1$. In this paper we verify numerically the existant theory for $1 < l < \infty$ where the Schwarz derivative of $f_h(x) = h\Lambda_l(x)$ is negative, see [12, 17]. Specially, we study the stability window of the first fixed point and how it evolves when $l \to \infty$ (Section 5). When $0 < l < 1$ there is no theory and in this work we do only a numerical exploration about this case. The conjectures made in this paper for the cases $0 < l < 1$ and $l \to \infty$ are based on numerical experiments.

To our knowledge only theory about the limit $l \to \infty$ is given by the Feigenbaum scaling constants $\delta_l = \lim_{j\to\infty} \frac{h_j - h_{j-1}}{h_{j+1} - h_j}$, $\delta_2 \approx 4.669$ and $\alpha_l = \lim_{l\to\infty} \frac{d_j}{d_{j+1}}$, $\alpha_2 \approx -2.503$ computed in [1, 2] where h_j is the first value h where a 2^j-period appears on the Feigenbaum's route to chaos and d_j is the value of the nearest cycle element to 0. The asymptotic values $\alpha_1, \alpha_\infty = -1$ (resp. $\delta_1 = 2$, $\lim_{l\to\infty} \delta_l \approx 30$) were proved in [7] (resp. [6, 18]). In [8] it was shown that $29.5128 < \delta_l < 29.9571$ for l large enough and the estimate $\delta_\infty = 29.576303 \pm 10^{-6}$ is given in [2, p.35].

The organisation of the paper is as follows. In Section 2, we recall some generalities about the logistic equation given by $f_h(x) = h\Lambda_l(x)$. A theoretical study for $l \in \{1, 2, 3, 4, 5\}$ is presented in Section 3 where the exact analytic solutions of (2) are described together with the Picard iterations and wavetracks. Section 4 presents new and surprising results for l far from the classical value $l = 2$. This is illustrated for the cases $0 < l < 1$ and l large. The relative evolution involving the three numbers 0, 1 and their mean value $\frac{1}{2}$ in the fixed point equation (2) is interpreted in Section 5. Finally some conclusions are given in Section 6.

§2. Logistic equations

Equation (2) is the family of logistic equations introduced in [12] which can be written as $x = h\Lambda_l(x)$ where the function

$$\Lambda_l(x) = 1 - |2x - 1|^l$$

is a continuous function with varying parameter $l > 0$. The maximum value 1 is attained at $x = \frac{1}{2}$ where l quantifies the smoothness of the function Λ_l.

There are two real functions $h \mapsto x(h, l)$ which solve (2), one is given by $\mathbf{0}$ and the other function $h \mapsto x(h)$ is called the *homogenisation path*, a term which will be explained in Section 5.

The family $f_h(x) = h\Lambda_l(x)$ has a negative Schwarz derivative when $l > 1$, thus it has observable periods, see [12, chapter 3]. The Picard iteration

$$x_0 = \tfrac{1}{2}, \quad x_{n+1} = f_h(x_n), \quad n \geq 0, \quad h \geq 0 \tag{3}$$

reveals the numerical behaviour of the law of composition repeatedly applied to f_h. Given an initial point x_0, it is possible to reach or not a fixed point after some iterations depending on h. The information provided by (3) is given by the *orbit diagram*.

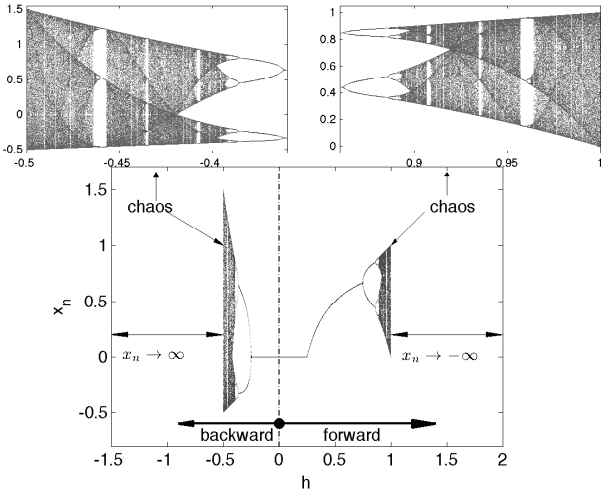

Figure 1: Logistic map: $x = h\Lambda_2(x) = 4hx(1 - x)$

An example is displayed for $l = 2$ in Figure 1, which is the well-known logistic map studied between 1970 and 1990, see [9, 10, 12]. The forward and backward orbit diagrams correspond to $h > 0$ and $h < 0$ respectively, they are shown in Figure 1. The complete diagram is displayed in the center; the top corners show the enlarged chaotic parts. We can observe that $|x_n(h)| \not\to \infty$ if $h \in [-\frac{1}{2}, 1]$.

At this point, a remark is in order. Most studies of (3) for $l = 2$ do not take into account the "backward" chaos obtained for $h \in [-\frac{1}{2}, -\frac{1}{4}]$ and focus exclusively on the "forward" one

obtained for $h \in [\frac{3}{4}, 1]$. From a computational point of view we shall see that this restriction is misleading when l positive evolves *away from 2*, either being large ($l \to \infty$) or small ($l \to 0$) (Section 4).

For $l = 2$, theory tells us that iteration (3) diverges as h varies in $\mathbb{R}$, unless h belongs to a finite interval. There are three ways in which $x_n(h)$ stays finite in (3) as $n \to \infty$:

1. $x_n(h)$ tends to a finite limit, $h \in]-\frac{1}{2}, \frac{3}{4}[$ in Figure 1,
2. $x_n(h)$ tends to belong to a periodic k-cycle, $k \geq 2$, see for instance the 2^k-cycles points for $h \in]-0.39, -\frac{1}{4}[$ and $h \in]\frac{3}{4}, 0.89[$ and the 3-cycle for $h \in]-0.46, -0.454[$ and $h \in]0.954, 0.96[$ in Figure 1,
3. $x_n(h)$ has no limit, but remains constrained to a finite interval as it can be observed in the chaotic parts in Figure 1.

In the following sections, we study the solutions of equation (2) and the portrait of the Picard iterations which remain finite as $n \to \infty$.

§3. Exponent $l \in \{1, 2, 3, 4, 5\}$

In this section we study the case where the positive exponent l in (2) is an integer ≤ 5. We look for real solutions $x(h) \neq 0$ for equation (2), we describe the Picard iterations given by (3) and we introduce the so called *wavetracks*.

3.1. Analytic solutions

To solve equation (2) is equivalent to find the roots of a polynomial if l is even or to find the roots of a piecewise polynomial if l is odd. In Table 1, we summarise the closed form of the exact real solutions developed in [14, Section 2] which come from solving the polynomials in (2) for $l \in \{1, 2, 3, 4\}$ when $x \in \mathbb{R}$ and for $l = 5$ when $x \leq \frac{1}{2}$. It can be easily seen that $\mathbf{0}$ is a solution to (2) for all $l > 0$. The real solutions which are different from $\mathbf{0}$ are plotted in Figure 2 (a) in the window $[-2, 2] \times [-1.5, 2.5]$ and in (b) in the window $[0.3, 0.7]^2$. For all other l, the analytic solution can be found by computing the inverse map $x \mapsto h(x) = \frac{x}{1-|2x-1|^l}$.

l		polynomial equation	
2		$x(x + (\frac{1}{4h} - 1)) = 0$	$\{x = 0, x = 1 - \frac{1}{4h}\}$
3	$x \leq \frac{1}{2}$	$x(8x^2 - 12x + 6 - \frac{1}{h}) = 0$	$\{x = 0, x = \frac{1}{4}(3 + \sqrt{\frac{2}{h} - 3})\}$
	$x > \frac{1}{2}$	$4x^3 - 6x^2 + (\frac{1}{2h} + 3)x - 1 = 0$	Cardano's method [14]
4		$x(2x^3 - 4x^2 + 3x + \frac{1}{8h} - 1) = 0$	Cardano's method [14]
5	$x \leq \frac{1}{2}$	$x(x^4 - \frac{5}{2}x^3 + \frac{5}{2}x^2 - \frac{5}{4}x + \frac{5}{16} - \frac{1}{32h}) = 0$	Ferrari's method [14]

Table 1: Solving $x = h\Lambda_l(x)$ by radicals

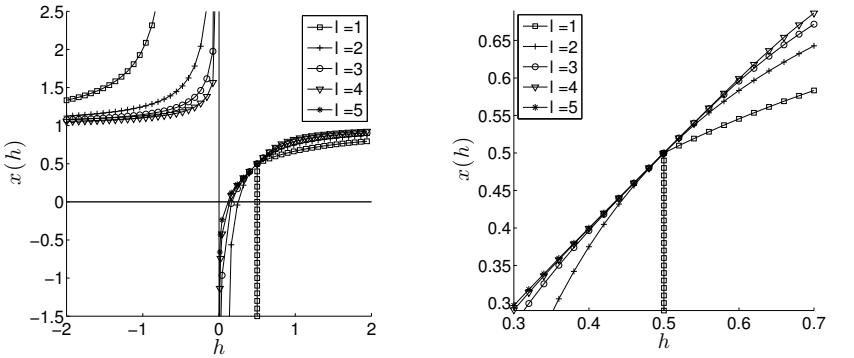

(a) Window $[-2, 2] \times [-1.5, 2.5]$ (b) Homogenisation path around $(\frac{1}{2}, \frac{1}{2})$

Figure 2: Analytic solution $x(h)$

3.2. Picard iterations

The general form of the Picard iterations (3) when $f_h(x) = h(1 - |2x - 1|^l)$ and $l \in \{2, 3, 4, 5\}$ is illustrated for $l = 4$ in the first row of Figure 3 (a), where $x_0 = \frac{1}{2}$ and the index n for the plotted iterates x_n varies between 200 and 400. The complete set of figures can be found in [14]. The windows containing chaos shrink as l is increased. In the second row of Figure 3 (a), the Picard iterations are plotted together with the analytic solution $x(h)$ as a dashed line. It can be observed that a part of the analytic solution $x(h)$ different from $\mathbf{0}$ is attained by the Picard iterations between ($h = \frac{1}{8}$, $x = 0$) and the first bifurcation from period 1 to 2 on the forward chaos around ($h = 0.83$, $x = 0.765$). The analytic solution equal to zero is reached between the first bifurcation point on the backward chaos around ($h = -0.12$, $x = 0$) and ($h = \frac{1}{8}$, $x = 0$). A similar behaviour is also observed for $l \in \mathbb{N}$, $l \geq 2$. By setting $x = 0$ in the equation $2x^3 - 4x^2 + 3x + \frac{1}{8h} - 1 = 0$ of Table 1 when $l = 4$ we obtain the point ($h = \frac{1}{8}$, $x = 0$). The points ($h \approx 0.83$, $x \approx 0.765$) and ($h \approx -0.12$, $x = 0$) are obtained experimentally.

3.3. Wavetracks

The wavetracks are the successive iterates by $h\Lambda_l$ of the critical point $x = \frac{1}{2}$. They are defined in [3, chapter 6] as follows:

$$\begin{cases} w_1(h) = h\Lambda_l(\frac{1}{2}), \\ w_k(h) = h\Lambda_l(w_{k-1}(h)), \quad k \geq 2. \end{cases} \tag{4}$$

The definition (4) is an extension of the "supertrack" curves studied in [13] for $l = 2$. According to (4), $w_1 = \mathbf{1}$ for all $l > 0$, and $w_2(h) = h(1 - |2h - 1|^l)$ which depends on l and satisfies $w_2(0) = w_2(1) = 0$, $w_2(\frac{1}{2}) = \frac{1}{2} = w_1(\frac{1}{2}) = x(\frac{1}{2})$. See Figure 4 where w_1 and w_2 are plotted with an asterisk marker and a square marker respectively. The numerical simulations displayed in Figure 4 confirm that for all n, the wavetracks exactly confine the chaos. If $h \in [\frac{1}{2}, 1]$, straightforward calculation shows that $w_2(h) \leq x_n(h) \leq w_1(h) = h$ and if $h \leq h_0$, then $w_1(h) \leq x_n(h) \leq w_2(h)$ where h_0 is such that $x(h_0) = 0$. In the third row of Figure 4 the

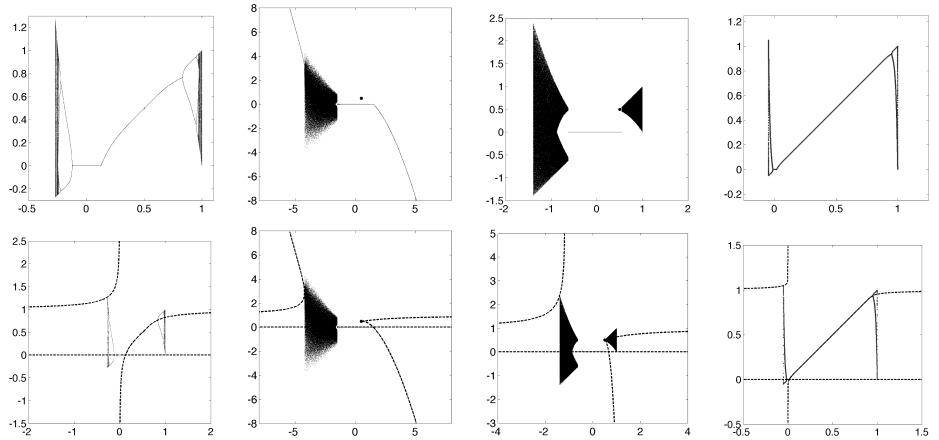

(a) $l = 4$ (b) $l = \frac{1}{3}$ (c) $l = \frac{3}{4}$ (d) $l = 32$

Figure 3: Picard iterations and exact $x(h)$ (dashed line)

first four wavetracks are plotted for $l = 4$. The wavetracks are found to be smooth for $l \in \mathbb{N}$, $l > 1$.

§4. Numerical simulations for l positive

In this section we describe experimental results for $0 < l < 1$ or l large and $l \to \infty$. In the absence of available theory, we propose some conjectures. The numerical simulations related to equation (2) when $0 < l < 1$ differ considerably from those of $l > 1$. The case $l = 1$ is the well-known *tent map*, studied in [12] and [3, chapter 6]. In [14, Section 5] we observed some peculiar phenomena for $0 < l < 1$ which we summarise in the following section.

4.1. $0 < l < 1$

For $0 < l \leq \tilde{l}$, $\tilde{l} \approx 0.502$, we observe that the iterates do not escape to $\pm\infty$ and there is no forward chaos, which is only replaced by the single point $(\frac{1}{2}, \frac{1}{2})$. The value 0.502 is experimentally obtained, see [14, Fig. 20]. Moreover x_n converges to $x(h)$ for $h \geq 1$, see for example the second column in Figure 3 (b) where $l = \frac{1}{3}$. The emergence of forward chaos near $h = 1$ occurs when l is around $\frac{1}{2}$ and when $\frac{1}{2} < l \leq 1$ the forward chaos expands gradually for $h \in [\frac{1}{2}, 1]$. The sharp difference in behaviour between $l < \tilde{l}$ and $l > \tilde{l}$, $\tilde{l} \approx 0.502$, can be appreciated when comparing second column where $l = \frac{1}{3}$ and the third row where $l = \frac{3}{4}$ in Figure 3.

The exact solutions $x(h)$ are plotted as a dashed line together with the Picard iterations in in the second row of Figure 3 (b) and (c). One solution is $\mathbf{0}$ and the other is found by using the inverse map $x \mapsto h = \frac{x}{1-|2x-1|^l}$. This function presents a cusp in $(\frac{1}{2}, \frac{1}{2})$. For $0 < l \leq \tilde{l}$, the exact solution $x = 0$ is attained by the Picard iteration between the emergence of the backward

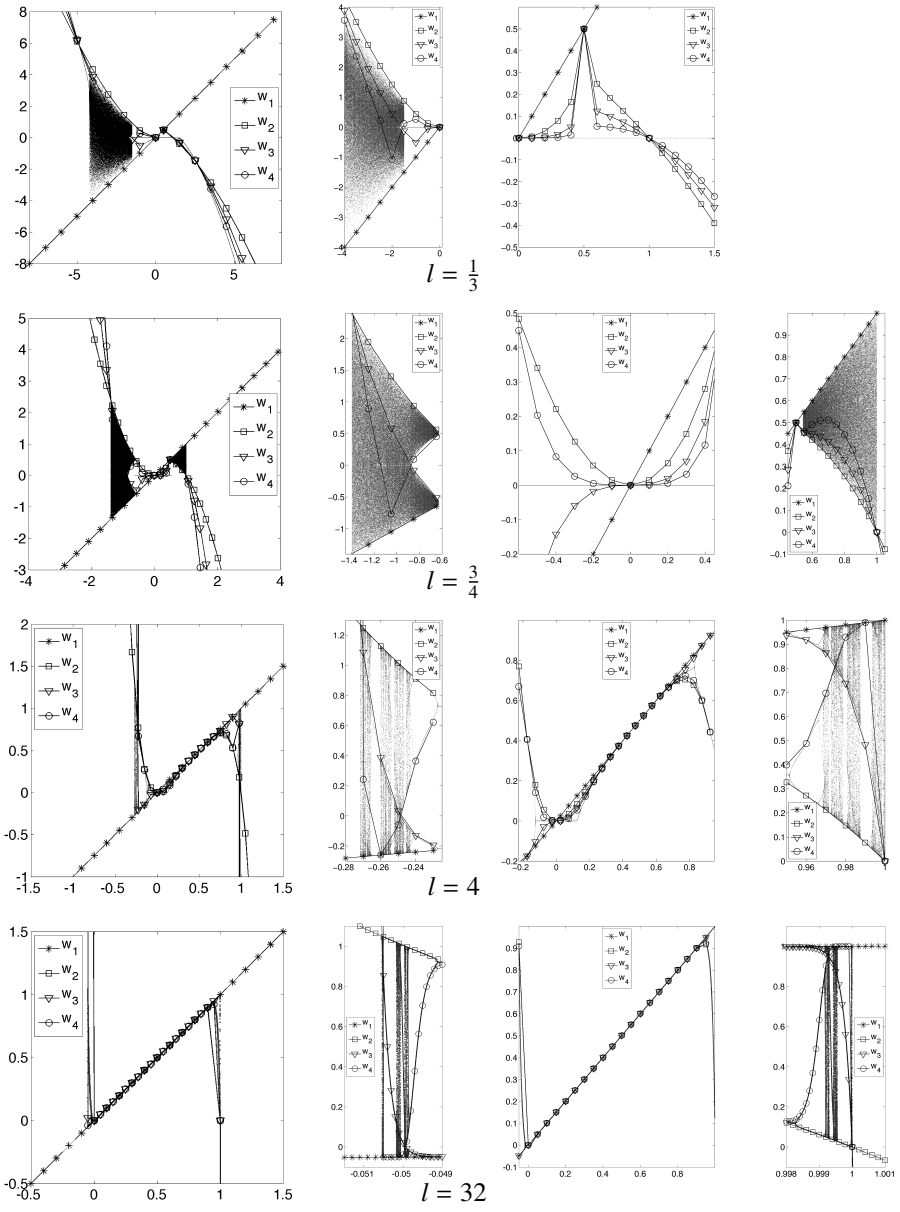

Figure 4: Wavetracks

chaos and $\tilde{h}$, ($\tilde{h}$ is such that $x(\tilde{h}) = 0$). Moreover, the two branches on the orbit map where $h > \tilde{h}$ and $h < h^*$, (h^* is the end of the backward chaos), coincide also with the exact $x(h)$. For $\tilde{l} < l \leq 1$, the Picard iterations attain the solution $\mathbf{0}$ only between the emergence of the

backward chaos and $\tilde{h}$. There is also a coincidence between $x(h)$ and the Picard iterations at the point $(\frac{1}{2}, \frac{1}{2})$ where $x(h)$ presents a cusp.

The numerical experiments on the wavetracks for $0 < l < 1$ are exemplified in the first and the second row of Figure 4 where the first 4 wavetracks are plotted together with the Picard iterations for $l = \frac{1}{3}$ and $l = \frac{3}{4}$. We can see that the wavetracks are continuous but not everywhere smooth and that the first two wavetracks confine the chaos. However for $0 < l < \tilde{l}$, the lower and upper bounds ($w_1 = h$ and $w_2(h) = h(1 - |2h - 1|^l)$) are not reached by x_n in the region of the backward chaos. See the first row of Figure 4 for $l = \frac{1}{3} < \tilde{l}$. The phenomenon disappears for $l = \frac{3}{4} > \tilde{l}$ (second row of Figure 4). This contrasts with the case $1 < l < \infty$ described in Section 3.3.

4.2. l is large

The behaviour of the logistic equation (2) when l is large, is illustrated in Figure 3 (d) when $l = 2^5 = 32$. We can see that the window of stability $[h_0, h_1]$ for $x(h)$ increases to cover the open interval $]0, 1[$ where h_0 is such that $x(h_0) = 0$ and h_1 is the first bifurcation from period 1 to 2, see Figure 3 (d) and also the third image in the fourth row of Figure 4. We conjecture that in the limit $l \to \infty$, the iterates do not escape to $\pm\infty$ if and only if $h \in [0, 1]$, they vary in $[0, 1]$ for $h = 0$ and 1 and describe the segment $x = h$ for $h \in]0, 1[$. Furthermore, we also observe that on $]0, 1[$ $w_2(h) \to h = w_1(h)$ as $l \to \infty$, see for instance the first and the third images of the fourth row of Figure 4, when $l = 32$. In the limit $l \to \infty$, the backward (resp. forward) chaos manifests itself as the axis $h = 0$, $x > 0$ (resp. $h = 1$, $x < 1$).

§5. Relative evolution of the numbers 0 and 1

The relative evolution of numbers 0 and 1 announced in the title of this work is revealed by the study of the fixed point equation (2). Equation (2) is satisfied if and only if

$$E^l(x) = 1 - \frac{x}{h}$$

where $E(x) = |2x - 1| = \frac{|x-1/2|}{1/2}$ is the relative distance of x to the mean value $\frac{1}{2}$. $E^l(x)$ measures the *degree of heterogeneity* between x and h. If $\frac{x}{h}$ gets close to 1 we say that there is a *symbiosis* between, or an *assimilation* of, the variables x and h, thus the map $h \mapsto x(h)$ which satisfies equation (2) and differs from $\mathbf{0}$ gets close to the identity map $\mathbf{1} : h \mapsto x = h$ and for this reason we call the function the *homogenisation path*. In Figure 2 (b) we observe that the approximation of the identity function $\mathbf{1}$ around $(\frac{1}{2}, \frac{1}{2})$ gets better as l increases. This situation is confirmed in Figure 3 (d) where $l = 32$. Furthermore, the Picard iterations in the first row of Figure 3 (a) and Figure 3 (d) show that through consecutive compositions there is an evolution and the identity function (which is the first wavetrack) is reached in the limit $n \to \infty$ on an increasing open interval in $]0, 1[$, as l increases, see the third image of the third of the fourth row in Figure 4. As $l \to \infty$, we conjecture that the interval tends to $]0, 1[$.

Another model for numerical evolution of the fixed points 0 and 1 is given by the following family of logistic equations

$$y = 1 - m|y|^l, \quad l > 0, \quad m \in \mathbb{R} \tag{5}$$

which appears in [1]. In this case the distance $|y|$ from y to 0 raised to the power l, is equal to the relative distance $\frac{1-y}{m}$, that is $|y|^l = \frac{1-y}{m}$, $m \neq 0$. Here $|y|$ is an absolute distance to 0 and the information in (5) is provided by 0 and 1 only, thus (5) gives an absolute evolution for the numbers 0 and 1 in contrast to the relative evolution given by (2). A detailed analysis of (5) and a comparison with (2) can be found in [16].

§6. Conclusions

The analysis of equation (2) by means of the Picard iteration, the exact solution and the wavetracks has allowed us to exemplify that around $(\frac{1}{2}, \frac{1}{2})$, $f_h(x) = h\Lambda_l(x)$ converges to the fixed point $\mathbf{1}$ of $f \circ f = f$ when $l \to \infty$ for $h \in]0, 1[$ except at the endpoints of this interval.

The *unexpected* behaviour for $0 < l < \tilde{l} \approx 0.502$ deserves more theoretical study. One solution to (2) is given by $\mathbf{0} = 0$ and the other satisfies $x = h$ for $h = \frac{1}{2}$ only. However thanks to the dynamics between the numbers 0, 1 and $\frac{1}{2}$ present in (2) the concept of unit 1 over $\mathbb{R}$ evolves into the identity function $\mathbf{1}$ over $C^0(\mathbb{R})$ when $\times$ is replaced by $\circ$, while 0 remains invariant ($\mathbf{0} = 0$). This dynamic evolution is provided by the introduction of the parameter h. The epistemological significance of the different behaviours of (2) and (5) is discussed in [5].

Acknowledgements

The author is grateful for the financial support from the Scientific Direction TOTAL through the contract DS-2755-B with Cerfacs (Qualitative Computing group). The author would also like to thank F. Chatelin for helpful scientific discussions.

The Cerfacs reports are available from *http://www.cerfacs.fr/algor/publications/*

References

[1] Briggs, K. A precise calculation of the Feigenbaum constants. *Mathematics of Computation 57*, 195 (1991), 435–439.

[2] Briggs, K. M. *Feigenbaum scaling in discrete dynamical systems*. PhD thesis, department of mathematics, University of Melbourne, 1997.

[3] Chatelin, F. *Qualitative Computing: a computational journey into nonlinearity*. World Scientific, Singapore, 2012.

[4] Chatelin, F., Latre, J. B., Rincon-Camacho, M. M., and Ricoux, P. Beyond and behind linear algebra. Tech. rep., CERFACS TR/PA/14/80, 2014.

[5] Chatelin, F., and Rincon-Camacho, M. M. Organic Information Theory: living and feeling beyond the boolean world. (In preparation). (2015).

[6] Collet, P., Eckmann, J.-P., and Lanford III, O. Universal properties of maps on an interval. *Communications in Mathematical Physics 76*, 3 (1980), 211–254.

[7] Delbourgo, R. Relations between universal scaling constants in dissipative maps. *Nonlinear dynamics and chaos, Fourth Physics Summer School, Canberra 1991* (1992), 231–256.

[8] Eckmann, J.-P., and Epstein, H. Bounds on the unstable eigenvalue for period doubling. *Communications in Mathematical Physics 128*, 2 (1990), 427–435.

[9] Feigenbaum, M. J. The universal metric properties of nonlinear transformations. *Journal of Statistical Physics 21*, 6 (1979), 669–706.

[10] May, R. M., et al. Biological populations with nonoverlapping generations: stable points, stable cycles, and chaos. *Science 186*, 4164 (1974), 645–647.

[11] McCarthy, P. J. Functional n^{th} roots of unity. *The Mathematical Gazette* (1980), 107–115.

[12] Nagashima, H., and Baba, Y. *Introduction to Chaos: Physics and Mathematics of Chaotic Phenomena*. IOP Publ., Bristol, UK, 1999.

[13] Oblow, E. Supertracks, supertrack functions and chaos in the quadratic map. *Physics Letters A 128*, 8 (1988), 406–412.

[14] Rincon-Camacho, M. M., Chatelin, F., and Ricoux, P. About a family of logistic equation based on a relative distance to $\frac{1}{2}$ raised to a positive power. Tech. rep., CERFACS TR/PA/14/55, 2014.

[15] Rincon-Camacho, M. M., Chatelin, F., and Ricoux, P. About relative and absolute logic evolutions under laws of degree 2 and 4 and in 4 dimensions at most. Tech. rep., CERFACS TR/PA/14/75, 2014.

[16] Rincon-Camacho, M. M., Chatelin, F., and Ricoux, P. Beyond Boolean logic. A family of logistic equations as a model for numerical evolution of the fixed points 0 and 1 for multiplication. Tech. rep., CERFACS TR/PA/14/68, 2014.

[17] Strogatz, S. H. *Nonlinear dynamics and chaos: with applications to physics, biology and chemistry*. Perseus publishing, 2001.

[18] Van Der Weele, J., Capel, H., and Kluiving, R. On the scaling factors $\alpha(z)$ and $\delta(z)$. *Physics Letters A 119*, 1 (1986), 15–20.

M. M. Rincon-Camacho
CERFACS
42, avenue Gaspard Coriolis,
31057 Toulouse, France
rincon@cerfacs.fr